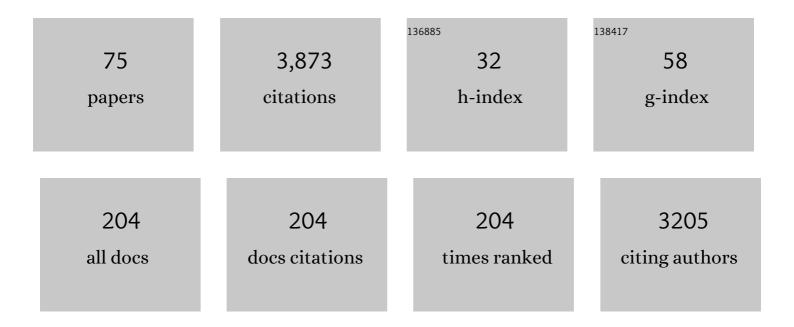
## Steffen Beirle

List of Publications by Year in descending order

Source: https://exaly.com/author-pdf/5839479/publications.pdf Version: 2024-02-01



STEEFEN REIDLE

#	Article	IF	CITATIONS
1	Megacity Emissions and Lifetimes of Nitrogen Oxides Probed from Space. Science, 2011, 333, 1737-1739.	6.0	402
2	Simultaneous global observations of glyoxal and formaldehyde from space. Geophysical Research Letters, 2006, 33, .	1.5	265
3	Improving algorithms and uncertainty estimates for satellite NO <sub>2</sub> retrievals: results from the quality assurance for the essential climate variables (QA4ECV) project. Atmospheric Measurement Techniques, 2018, 11, 6651-6678.	1.2	187
4	The Monte Carlo atmospheric radiative transfer model McArtim: Introduction and validation of Jacobians and 3D features. Journal of Quantitative Spectroscopy and Radiative Transfer, 2011, 112, 1119-1137.	1.1	174
5	NO <sub><i>x</i></sub> lifetimes and emissions of cities and power plants in polluted background estimated by satellite observations. Atmospheric Chemistry and Physics, 2016, 16, 5283-5298.	1.9	168
6	Tropospheric NO <sub>2</sub> vertical column densities over Beijing: results of the first three years of ground-based MAX-DOAS measurements (2008–2011) and satellite validation. Atmospheric Chemistry and Physics, 2013, 13, 1547-1567.	1.9	149
7	NO <sub><i>x</i></sub> emission trends over Chinese cities estimated from OMI observations during 2005 to 2015. Atmospheric Chemistry and Physics, 2017, 17, 9261-9275.	1.9	146
8	Structural uncertainty in air mass factor calculation for NO <sub>2</sub> and HCHO satellite retrievals. Atmospheric Measurement Techniques, 2017, 10, 759-782.	1.2	133
9	Algorithm theoretical baseline for formaldehyde retrievals from S5P TROPOMI and from the QA4ECV project. Atmospheric Measurement Techniques, 2018, 11, 2395-2426.	1.2	127
10	Pinpointing nitrogen oxide emissions from space. Science Advances, 2019, 5, eaax9800.	4.7	100
11	In situ, satellite measurement and model evidence on the dominant regional contribution to fine particulate matter levels in the Paris megacity. Atmospheric Chemistry and Physics, 2015, 15, 9577-9591.	1.9	92
12	Estimating the volcanic emission rate and atmospheric lifetime of SO <sub>2</sub> from space: a case study for Kīlauea volcano, Hawai`i. Atmospheric Chemistry and Physics, 2014, 14, 8309-8322.	1.9	87
13	Ground-based MAX-DOAS observations of tropospheric aerosols, NO <sub>2</sub> , SO <sub>2</sub> and HCHO in Wuxi, China, from 2011 to 2014. Atmospheric Chemistry and Physics, 2017, 17, 2189-2215.	1.9	86
14	Validation of OMI, GOME-2A and GOME-2B tropospheric NO <sub>2</sub> , SO <sub>2</sub> and HCHO products using MAX-DOAS observations from 2011 to 2014 in Wuxi, China: investigation of the effects of priori profiles and aerosols on the satellite products. Atmospheric Chemistry and Physics, 2017, 17, 5007-5033.	1.9	81
15	Improved slant column density retrieval of nitrogen dioxide and formaldehyde for OMI and GOME-2A from QA4ECV: intercomparison, uncertainty characterisation, and trends. Atmospheric Measurement Techniques, 2018, 11, 4033-4058.	1.2	74
16	Systematic investigation of bromine monoxide in volcanic plumes from space by using the GOME-2 instrument. Atmospheric Chemistry and Physics, 2013, 13, 4749-4781.	1.9	69
17	MAX-DOAS measurements and satellite validation of tropospheric NO2 and SO2 vertical column densities at a rural site of North China. Atmospheric Environment, 2016, 133, 12-25.	1.9	66
18	Cloud detection and classification based on MAX-DOAS observations. Atmospheric Measurement Techniques, 2014, 7, 1289-1320.	1.2	63

STEFFEN BEIRLE

#	Article	IF	CITATIONS
19	A multi-site intercomparison of integrated water vapour observations for climate change analysis. Atmospheric Measurement Techniques, 2014, 7, 2487-2512.	1.2	61
20	Abrupt recent trend changes in atmospheric nitrogen dioxide over the Middle East. Science Advances, 2015, 1, e1500498.	4.7	59
21	Parameterizing the instrumental spectral response function and its changes by a super-Gaussian and its derivatives. Atmospheric Measurement Techniques, 2017, 10, 581-598.	1.2	58
22	Intercomparison of aerosol extinction profiles retrieved from MAX-DOAS measurements. Atmospheric Measurement Techniques, 2016, 9, 3205-3222.	1.2	53
23	Global patterns of lightning properties derived by OTD and LIS. Natural Hazards and Earth System Sciences, 2014, 14, 2715-2726.	1.5	52
24	Total column water vapour measurements from GOME-2 MetOp-A and MetOp-B. Atmospheric Measurement Techniques, 2015, 8, 1111-1133.	1.2	43
25	Re-evaluating the NO <sub>2</sub> hotspot over the South African Highveld. South African Journal of Science, 2012, 108, .	0.3	42
26	Absolute calibration of the colour index and O <sub>4</sub> absorption derived from Multi AXis (MAX-)DOAS measurements and their application to a standardised cloud classification algorithm. Atmospheric Measurement Techniques, 2016, 9, 4803-4823.	1.2	42
27	A methodology to constrain carbon dioxide emissions from coal-fired power plants using satellite observations of co-emitted nitrogen dioxide. Atmospheric Chemistry and Physics, 2020, 20, 99-116.	1.9	40
28	GOME Observations of Stratospheric Trace Gas Distributions during the Splitting Vortex Event in the Antarctic Winter of 2002. Part I: Measurements. Journals of the Atmospheric Sciences, 2005, 62, 778-785.	0.6	38
29	A global aerosol classification algorithm incorporating multiple satellite data sets of aerosol and trace gas abundances. Atmospheric Chemistry and Physics, 2015, 15, 10597-10618.	1.9	38
30	Catalog of NO <sub><i>x</i></sub> emissions from point sources as derived from the divergence of the NO <sub>2</sub> flux for TROPOMI. Earth System Science Data, 2021, 13, 2995-3012.	3.7	37
31	Detection of water vapour absorption around 363†nm in measured atmospheric absorption spectra and its effect on DOAS evaluations. Atmospheric Chemistry and Physics, 2017, 17, 1271-1295.	1.9	36
32	Intercomparison of MAX-DOAS vertical profile retrieval algorithms: studies using synthetic data. Atmospheric Measurement Techniques, 2019, 12, 2155-2181.	1.2	34
33	Intercomparison of MAX-DOAS vertical profile retrieval algorithms: studies on field data from the CINDI-2 campaign. Atmospheric Measurement Techniques, 2021, 14, 1-35.	1.2	32
34	Cloud and aerosol classification for 2.5 years of MAX-DOAS observations in Wuxi (China) and comparison to independent data sets. Atmospheric Measurement Techniques, 2015, 8, 5133-5156.	1.2	31
35	MAX-DOAS measurements of HONO slant column densities during the MAD-CAT campaign: inter-comparison, sensitivity studies on spectral analysis settings, and error budget. Atmospheric Measurement Techniques, 2017, 10, 3719-3742.	1.2	31
36	A feasibility study for the retrieval of the total column precipitable water vapour from satellite observations in the blue spectral range. Atmospheric Measurement Techniques, 2013, 6, 2593-2605.	1.2	30

## STEFFEN BEIRLE

#	Article	IF	CITATIONS
37	Validation of Aura-OMI QA4ECV NO <sub>2</sub> climate data records with ground-based DOAS networks: the role of measurement and comparison uncertainties. Atmospheric Chemistry and Physics, 2020, 20, 8017-8045.	1.9	29
38	Long-term MAX-DOAS measurements of NO <sub>2</sub> , HCHO, and aerosols and evaluation of corresponding satellite data products over Mohali in the Indo-Gangetic Plain. Atmospheric Chemistry and Physics, 2020, 20, 14183-14235.	1.9	28
39	The STRatospheric Estimation Algorithm from Mainz (STREAM): estimating stratospheric NO <sub>2</sub> from nadir-viewing satellites by weighted convolution. Atmospheric Measurement Techniques, 2016, 9, 2753-2779.	1.2	27
40	The Mainz profile algorithm (MAPA). Atmospheric Measurement Techniques, 2019, 12, 1785-1806.	1.2	27
41	Detection of Trends and Seasonal Variation in Tropospheric Nitrogen Dioxide over Pakistan. Aerosol and Air Quality Research, 2015, 15, 2508-2524.	0.9	27
42	Estimation of the Paris NO <sub><i>x</i></sub> emissions from mobile MAX-DOAS observations and CHIMERE model simulations during the MEGAPOLI campaign using the closed integral method. Atmospheric Chemistry and Physics, 2017, 17, 7853-7890.	1.9	26
43	Nitrogen oxides in the global upper troposphere: interpreting cloud-sliced NO <sub>2</sub> observations from the OMI satellite instrument. Atmospheric Chemistry and Physics, 2018, 18, 17017-17027.	1.9	25
44	Top-Down NOX Emissions of European Cities Based on the Downwind Plume of Modelled and Space-Borne Tropospheric NO2 Columns. Sensors, 2018, 18, 2893.	2.1	24
45	MAX-DOAS observations of the total atmospheric water vapour column and comparison with independent observations. Atmospheric Measurement Techniques, 2013, 6, 131-149.	1.2	23
46	Linearisation of the effects of spectral shift and stretch in DOAS analysis. Atmospheric Measurement Techniques, 2013, 6, 661-675.	1.2	23
47	Is a scaling factor required to obtain closure between measured and modelled atmospheric O <sub>4</sub> absorptions? An assessment of uncertainties of measurements and radiative transfer simulations for 2 selected days during the MAD-CAT campaign. Atmospheric Measurement Techniques, 2019, 12, 2745-2817.	1.2	22
48	Total column water vapour retrieval from S-5P/TROPOMI in the visible blue spectral range. Atmospheric Measurement Techniques, 2020, 13, 2751-2783.	1.2	22
49	New concepts for the comparison of tropospheric NO <sub>2</sub> column densities derived from car-MAX-DOAS observations, OMI satellite observations and the regional model CHIMERE during two MEGAPOLI campaigns in Paris 2009/10. Atmospheric Measurement Techniques. 2015. 8. 2827-2852.	1.2	20
50	Technical Note: Temporal change in averaging kernels as a source of uncertainty in trend estimates of carbon monoxide retrieved from MOPITT. Atmospheric Chemistry and Physics, 2013, 13, 11307-11316.	1.9	18
51	Vertical Profiles of Tropospheric Ozone From MAXâ€DOAS Measurements During the CINDIâ€⊋ Campaign: Part 1—Development of a New Retrieval Algorithm. Journal of Geophysical Research D: Atmospheres, 2018, 123, 10,637.	1.2	18
52	An improved total and tropospheric NO <sub>2</sub> column retrieval for GOME-2. Atmospheric Measurement Techniques, 2019, 12, 1029-1057.	1.2	18
53	Inter-comparison of MAX-DOAS measurements of tropospheric HONO slant column densities and vertical profiles during the CINDI-2 campaign. Atmospheric Measurement Techniques, 2020, 13, 5087-5116.	1.2	18
54	Multi-satellite sensor study on precipitation-induced emission pulses of NO <sub><i>x</i></sub> from soils in semi-arid ecosystems. Atmospheric Chemistry and Physics, 2016, 16, 9457-9487.	1.9	17

STEFFEN BEIRLE

#	Article	IF	CITATIONS
55	The ESA GOME-Evolution "Climate―water vapor product: a homogenized time series of H <sub>2</sub> O columns from GOME, SCIAMACHY, and GOME-2. Earth System Science Data, 2018, 10, 449-468.	3.7	16
56	An improved TROPOMI tropospheric NO <sub>2</sub> research product over Europe. Atmospheric Measurement Techniques, 2021, 14, 7297-7327.	1.2	16
57	In-operation field-of-view retrieval (IFR) for satellite and ground-based DOAS-type instruments applying coincident high-resolution imager data. Atmospheric Measurement Techniques, 2017, 10, 881-903.	1.2	12
58	A new method for inferring city emissions and lifetimes of nitrogen oxides from high-resolution nitrogen dioxide observations: a model study. Atmospheric Chemistry and Physics, 2022, 22, 1333-1349.	1.9	12
59	Evaluating different methods for elevation calibration of MAX-DOAS (Multi AXis Differential Optical) Tj ETQq1 Techniques, 2020, 13, 685-712.	1 0.784314 1.2	f rgBT /Over 11
60	Applications of Satellite Observations of Tropospheric Composition. Physics of Earth and Space Environments, 2011, , 365-449.	0.5	10
61	Seasonal variation of tropospheric bromine monoxide over the Rann of Kutch salt marsh seen from space. Atmospheric Chemistry and Physics, 2016, 16, 13015-13034.	1.9	10
62	Nitrogen dioxide decline and rebound observed by GOME-2 and TROPOMI during COVID-19 pandemic. Air Quality, Atmosphere and Health, 2021, 14, 1737-1755.	1.5	10
63	Profile information on CO from SCIAMACHY observations using cloud slicing and comparison with model simulations. Atmospheric Chemistry and Physics, 2014, 14, 1717-1732.	1.9	9
64	Global Spatiotemporal Variability of Integrated Water Vapor Derived from GPS, GOME/SCIAMACHY and ERA-Interim: Annual Cycle, Frequency Distribution and Linear Trends. Remote Sensing, 2022, 14, 1050.	1.8	8
65	Retrieval of tropospheric aerosol, NO <sub>2</sub> , and HCHO vertical profiles from MAX-DOAS observations over Thessaloniki, Greece: intercomparison and validation of two inversion algorithms. Atmospheric Measurement Techniques, 2022, 15, 1269-1301.	1.2	8
66	The tilt effect in DOAS observations. Atmospheric Measurement Techniques, 2017, 10, 4819-4831.	1.2	7
67	A new method for the absolute radiance calibration for UV–vis measurements of scattered sunlight. Atmospheric Measurement Techniques, 2015, 8, 4265-4280.	1.2	6
68	Technical note: Evaluation of profile retrievals of aerosols and trace gases for MAX-DOAS measurements under different aerosol scenarios based on radiative transfer simulations. Atmospheric Chemistry and Physics, 2021, 21, 12867-12894.	1.9	5
69	Identification of atmospheric and oceanic teleconnection patterns in a 20-year global data set of the atmospheric water vapour column measured from satellites in the visible spectral range. Atmospheric Chemistry and Physics, 2021, 21, 5315-5353.	1.9	4
70	Quantitative comparison of measured and simulated O <sub>4</sub> absorptions for one day with extremely low aerosol load over the tropical Atlantic. Atmospheric Measurement Techniques, 2021, 14, 3871-3893.	1.2	4
71	Observations of iodine monoxide over three summers at the Indian Antarctic bases of Bharati and Maitri. Atmospheric Chemistry and Physics, 2021, 21, 11829-11842.	1.9	3
72	MICRU: an effective cloud fraction algorithm designed for UV–vis satellite instruments with large viewing angles. Atmospheric Measurement Techniques, 2021, 14, 3989-4031.	1.2	2

#	Article	IF	CITATIONS
73	Evaluation of the coupled high-resolution atmospheric chemistry model system MECO(n) using in situ and MAX-DOAS NO <sub>2</sub> measurements. Atmospheric Measurement Techniques, 2021, 14, 5241-5269.	1.2	2
74	Estimating real driving emissions from multi-axis differential optical absorption spectroscopy (MAX-DOAS) measurements at the A60 motorway near Mainz, Germany. Atmospheric Measurement Techniques, 2021, 14, 769-783.	1.2	1
75	Calculating the vertical column density of O <sub>4</sub> during daytime from surface values of pressure, temperature, and relative humidity. Atmospheric Measurement Techniques, 2022, 15, 987-1006.	1.2	0